Dynamics of spatio-temporal defects in the Taylor-Dean system

P Bot, I Mutabazi

Eur. Phys. J. B **13**, 141–155 (2000)

THE EUROPEAN PHYSICAL JOURNAL B
EDP Sciences

Dynamics of spatio-temporal defects in the Taylor-Dean system

P. Bot[a] and I. Mutabazi[b]

Laboratoire de Mécanique, Université du Havre, BP 540, 76058 Le Havre Cedex, France

Received 23 February 1999 and Received in final form 26 May 1999

Abstract. The dynamics of defects in a pattern of traveling inclined rolls has been investigated. Two regimes were identified in the neighborhood of defects: a diffusive regime, with a negative phase diffusion coefficient, and a coalescence regime in which the phase gradient diverges in time following a power law behavior. The observed periodic nucleation of defects is related to the frequency inhomogeneity induced by the disymmetry of the wave amplitude. Amplitude holes have been observed in the secondary modulated pattern.

PACS. 47.20.-k Hydrodynamic stability – 47.20.Lz Secondary instability – 47.54.+r Pattern selection; pattern formation

1 Introduction

The study of spatially organized patterns in nonlinear dissipative extended systems has drawn much attention in recent years and has led to a better understanding of the transition to weak chaos in these systems. When a control parameter, which is a measure of an external constraint imposed on the system, is varied, the system is driven away far from equilibrium and a pattern emerges from the homogeneous state. The resulting spatially organized pattern may be either stationary or periodic in time. Spatially organized patterns have been observed in many systems ranging from hydrodynamic flows [1], nonlinear optics [2], liquid crystals, materials [3] to chemical reactions [4].

Some of the striking features of spatio-temporal patterns in extended systems are the emergence of defects due to long wavelength modulations and the occurrence of spatio-temporal chaos near the onset of the first transition. It is now commonly admitted that the dynamics of traveling waves patterns observed *via* a supercritical bifurcation in extended systems can be well described by the complex Ginzburg-Landau equation [1,5,6] commonly referred to as CGLE. A thourough phase diagram of different states from CGLE has been identified in numerical simulations [7–9]: stable waves, phase turbulence, defect turbulence, bichaotic regime and intermittent regime. The defect turbulence is characterized by the occurrence of defects (points of the pattern where the amplitude vanishes and phase is undefined). In the phase turbulence, the amplitude does not vanish but the integral mean wavenumber (also called *winding number*) is constant. The bichaotic regime is characterized by a mixed state of phase and defect turbulence. In the intermittent regime, defect turbulence and stable waves or phase turbulence appear alternatively at irregular time intervals and at different pattern positions. Away from the Benjamin-Feir line in the unstable regime, the complex Ginzburg-Landau equation admits amplitude hole solutions identified first by Nozaki-Bekki [7,10–12] and recently by van Hecke [13].

The topological or point defects have been reported in many experiments for example in binary mixture convection [14,15] and in the Taylor-Dean system [16]. Amplitude holes have been observed in recent experiments in convection in annulus [7,17–19].

The present paper is concerned with experimental results in which both defects and amplitude holes have been observed in patterns arizing in the Taylor-Dean system. The latter consists of the flow partially filling the gap between two horizontal coaxial cylinders with differential rotation. The bifurcations from the base flow state give rise to either traveling rolls or stationnary rolls depending on the rotation ratio between the cylinders [20]. When the outer cylinder is fixed, the primary state of the pattern arises from the base flow *via* a supercritical bifurcation and consists of traveling inclined rolls characterized by a well-defined wavenumber $q = 4.8$ and a drifting velocity that increases with the control parameter [16,20]. This transition is related to the broken reflection symmetry of the base state flow. The pattern pertains longwavelength modulations that induce a Benjamin-Feir instability in form of roll collisions. We have attempted a thourough characterization of these defects in the primary pattern. The secondary pattern is a spatio-temporally modulated pattern which consists of traveling triplets (group of 3 rolls) that can collide each other giving rise to defects and amplitude holes.

[a] *Present address*: Laboratoire d'Hydrodynamique, École Navale, 29240 Brest-Naval, France.
[b] e-mail: `mutabazi@cher.univ-lehavre.fr`

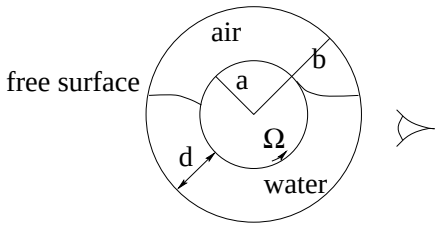

Fig. 1. Cross section of the experimental Taylor-Dean system.

The paper is organized as follows: in the second section we describe the experimental setup, in Section 3 we present results that will be discussed in Section 4 while Section 5 contains concluding remarks.

2 Description of the experiment

2.1 Experimental system

The Taylor-Dean configuration used in our experiments consists of two coaxial horizontal cylinders with a gap partially filled with water [21,22]. The inner cylinder is made of black anodized aluminium (for a better visualization contrast) with a radius $a = 4.46$ cm. The outer cylinder is made of glass with a radius $b = 5.08$ cm. The gap between the cylinders is $d = b - a = 0.62$ cm over a length $L = 55$ cm. Hence, the system has a radius ratio $\eta = \frac{a}{b} = 0.878$, and an aspect ratio $\Gamma = \frac{L}{d} = 90$. The filling level angle θ_f is chosen as $\theta_\mathrm{f}/2\pi = 0.7$ (Fig. 1).

The inner cylinder is rotated by a DC servomotor which is driven by a PC, while the outer cylinder remains fixed in the laboratory frame. Thus, the only control parameter is the Reynolds number relative to the inner rotating cylinder defined as $\mathrm{Re} = \Omega a d/\nu$, where Ω is the cylinder angular frequency and ν the kinematic viscosity of the fluid. The precision on the geometric dimensions and on the rotation frequency is 0.5%. Therefore, the main error on the control parameter Re comes from the viscosity fluctuations with temperature. During experiments, the temperature has been measured and we estimated the relative uncertainty on the control parameter to be $\Delta\mathrm{Re}/\mathrm{Re} \sim 1\%$.

Teflon rings are attached at the end of the inner surface of the fixed outer cylinder in order to reduce the effects of Ekman recirculation. The aspect ratio $\Gamma = 90$ is large enough to consider the experimental system as an extended system [5], actually more than 70 rolls are observed in the system.

We have used distilled water with 2% Kalliroscope AQ1000 for the visualization. With a light from a fluorescent tube, the flow was visualized on the front side. To obtain spatial information about the roll dynamics, a linear 1024-pixel charge coupled device (CCD) array records the reflected light intensity distribution $I(x)$ from a line parallel to the axis of the cylinders, 1 cm below the free surface. The recorded length is from 30 to 40 cm in the central part of the system, corresponding to a spatial resolution of 25 to 34 pixels /cm. The intensity is sampled in 256 values, displayed in grey levels at regular time intervals along time axis to produce space-time diagrams $I(x,t)$ of the pattern. For a good resolution of frequency spectra, acquisitions of 8192 time steps of 0.2 s were used. Wavenumber spectra have been averaged in time in order to improve their resolution. The data are processed on a UNIX workstation.

Times, lengths and velocities are scaled respectively by the radial diffusion time $d^2/\nu \sim 40$ s, the gap size d and the radial diffusion velocity $\nu/d \sim 0.016$ cm/s. All quantities used in this paper are dimensionless, unless stated differently. In experiments, in order to avoid spurious transient states, we waited 15 minutes between each variation of the control parameter, from 260 up to 340 by a step $\Delta\mathrm{Re} = 2$, while 30 minutes were required before each data acquisition.

2.2 Demodulation of the spatio-temporal signals

In order to quantify spatial and temporal variations of wavenumbers and frequencies, we have performed the demodulation technique by Hilbert Transform [7,18] of the signal with respect to time. The real signal $I(x,t)$ is transformed in its complex equivalent expression as follows:

$$I(x,t) = \Re\{|A(x,t)|\,\mathrm{e}^{\mathrm{i}\Phi(x,t)}\} \qquad (1)$$

where $\Re$ stands for the real part. In practice, the original signal $I(x,t)$ is first band-pass filtered in space with relatively large band (elimination of large-scale lighting inhomogeneities and small-scale noise). Then, a temporal Fast Fourier Transform is computed, and components of negative frequencies are set to zero with a smooth filter. The latter consists in a band-pass filter with a band carefully adapted to each pattern, centered on the rolls frequency. Afterwards, the inverse Fourier Transform of the truncated signal in the spectral space gives the amplitude $|A(x,t)|$ and the total phase $\Phi(x,t)$. The wavenumbers and frequencies are determined as the spatial and temporal phase gradients: $q(x,t) = \partial\Phi/\partial x$, $\omega(x,t) = 2\pi f = \partial\Phi/\partial t$.

3 Results

3.1 Sources and defects in the primary pattern

The first instability of the base flow is supercritical and occurs at the critical value of the control parameter $\mathrm{Re_c} = 260 \pm 2$ giving rise to a pattern of traveling inclined rolls: no hysteresis has been observed when ramping up and down. The rolls intensity vanishes slightly before the ends, suggesting that the roll pattern has soft boundaries, there is no reflection from the boundaries. This pattern has a wavenumber $q_\mathrm{c} = 4.8 \pm 0.1$ and a frequency $f_\mathrm{c} = 18.90 \pm 0.05$ corresponding to a drift velocity $v_\mathrm{d} = 24.7$ [21,22]. This space and time periodic pattern exhibits two kinds of defects: sources separating rolls traveling in opposite directions and instantaneous defects due to collisions between rolls (Fig. 2).

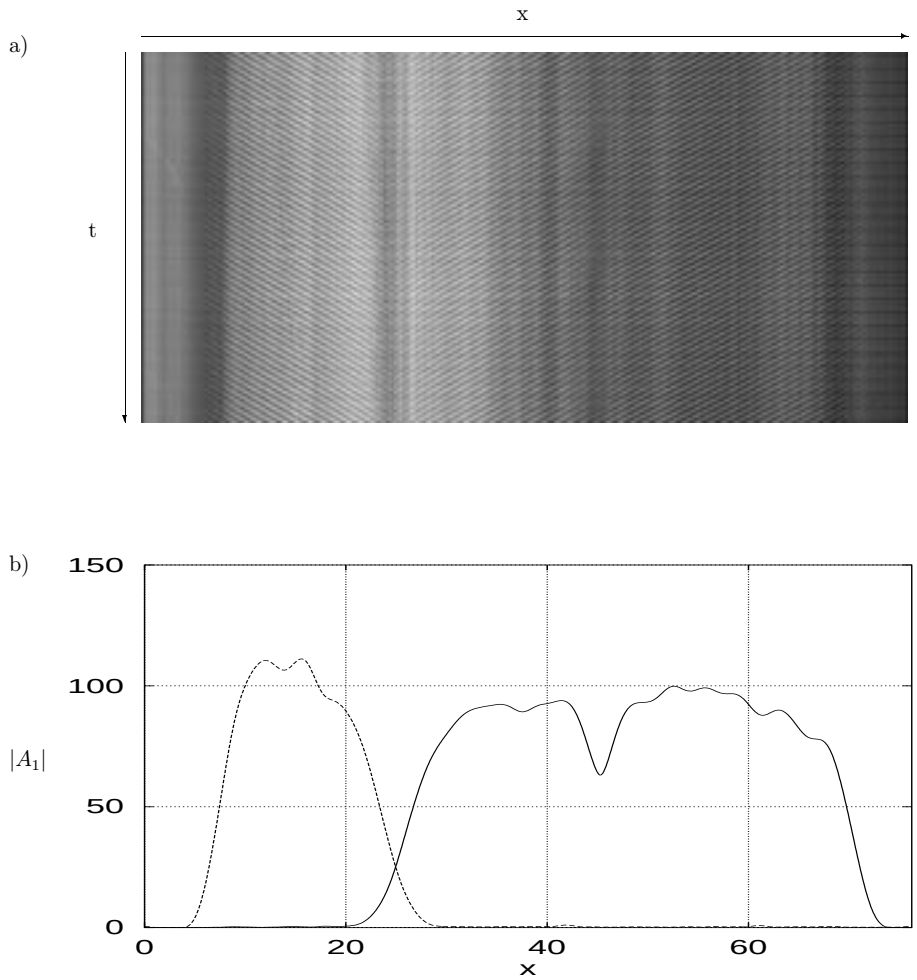

Fig. 2. a) Space-time diagram of the primary pattern at $\mathrm{Re} = 273$ with a source at $x_\mathrm{s} = 24.9$ and b) time-averaged amplitude profile of right (solid line) and left (dashed line) traveling waves.

3.1.1 Sources

When rolls appear, the rising pattern spontaneously breaks the reflection symmetry of the base state, and inclined rolls travel either to the right or to the left. Hence, there may exist sub-patterns traveling in opposite directions separated by sources or sinks. The number of these defects is very sensitive to the ramping rate: for a slow ramping rate ($\mathrm{dRe}/\mathrm{d}t < 0.1$), the pattern has always a single propagation direction at threshold, but a fast change of Re induces many sources and sinks. Moreover, even for a slow ramping rate, a source appears in the pattern (Figs. 2 and 3) for higher values of the control parameter *i.e.* for $\epsilon = (\mathrm{Re} - \mathrm{Re_c})/\mathrm{Re_c} \geq 0.05$. The source appears randomly in the pattern at any position which may change when the control parameter is varied abruptly. In a given run, with a slow ramping rate, the source fluctuates around a stable position.

The spatial profiles of the amplitude, wavenumber and frequency are stationary: in fact, their variations are less than 1% on the time scale of one hour ($\sim 100d^2/\nu$). We have determined the time averaged profiles of the amplitude, wavenumber and frequency of right and left traveling rolls (Fig. 3). The intersection of amplitude profiles allows us to define the position of the source core. The fluctuations observed on the amplitude profiles are due to inhomogeneous distribution of Kalliroscope flakes, and they are not relevant of the pattern amplitude. There is no significant difference between wavenumber of left and right traveling pattern, but the fluctuations of the wavenumber are within $\delta q = 0.25$. The frequency profile on each side of the source is flat but there is a frequency shift $\delta f = f_\mathrm{r} - f_\mathrm{l}$ between left and right traveling rolls. Rolls in the pattern with shorter axial extension drift faster than those within larger extension. The frequency shift depends on the source position in the pattern and vanishes when the source is in the center of the system, it might be due to a mean flow in the system. The source core consists of two counter-propagating waves with comparable amplitudes.

3.1.2 Defects

The defects spontaneously nucleate in the pattern in the range $\mathrm{Re} \in [261; 288]$ and consist of roll collisions leading to annihilation of one roll. Creation of roll is a rare event,

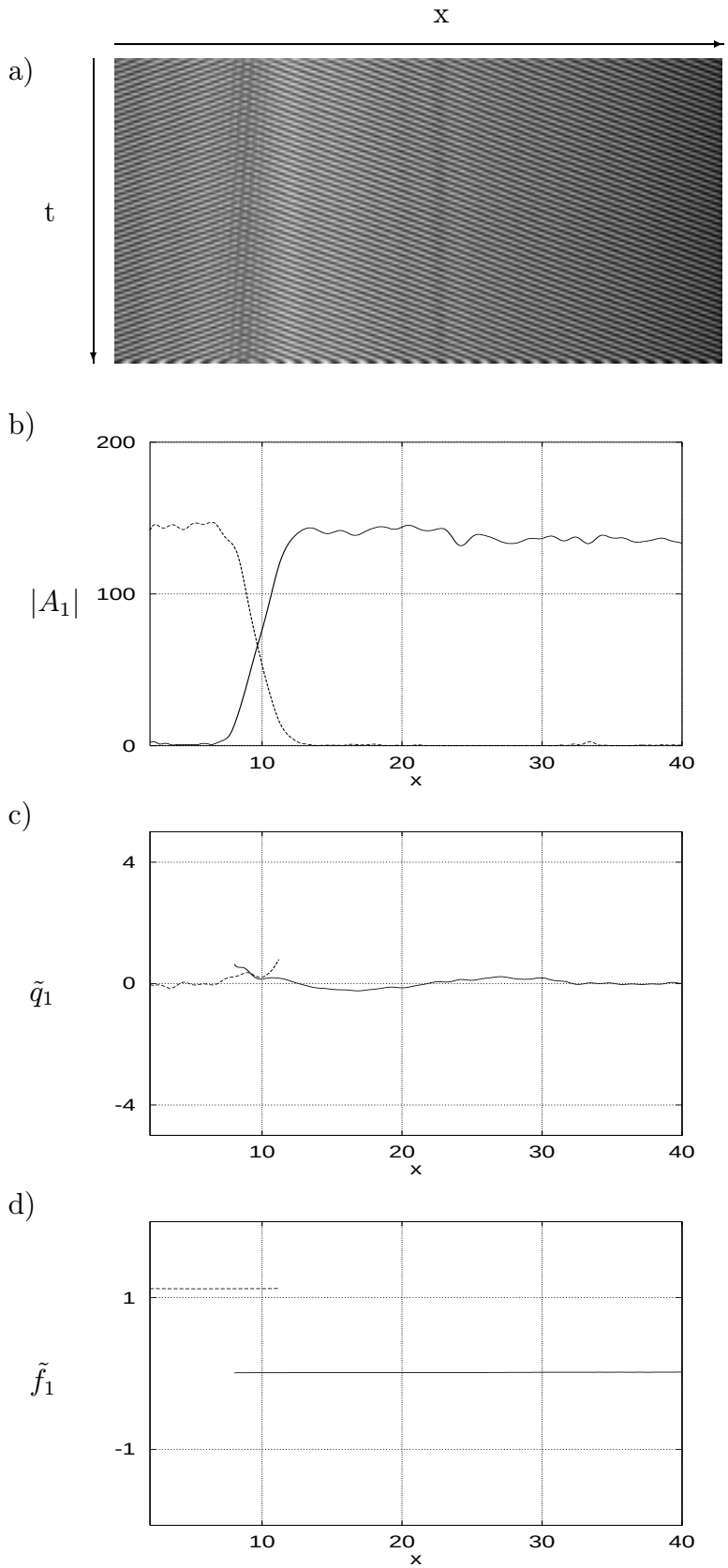

Fig. 3. a) Space-time diagram of the primary pattern at Re = 289 with a source at $x_s = 9.7$ (the pattern is shown over a time extension of 2.3) and time-averaged profile of the amplitude (b), the wavenumber (c) and the frequency (d) for right (solid line) and left (dashed line) traveling waves.

mostly observed after a sharp ramping in the control parameter, they are not studied here.

We have characterized the neighborhood of a defect (Figs. 4 and 5). Compression of the rolls accumulates, resulting in a slowly growing bump in the phase gradient profile and a slow decrease of the amplitude. This mechanism is amplified, and leads to a dramatic increase of a phase gradient peak and a sharp drop of the amplitude. The pattern cannot sustain such constraints and loses a roll (defect). In the defect core, the amplitude vanishes and the phase of the pattern jumps by 2π resulting in the discontinuity of spatial and temporal phase gradients. After the loss of the roll, the remaining rolls are expanded and there is a sharp dip of the phase gradient, which relaxes rapidly, while the amplitude increases. The source or edges feed the pattern with new rolls and the previous mechanism can be repeated.

We have observed that, the defects occur periodically in time at the same distance from the source within 2% (Figs. 6 and 7) for a given run. The distance at which the defects occur depends on the separation length betwen the source and the edge. The time between two consecutive defects at the same location is constant within 5% for a given pattern. The time averaged roll frequency exhibits a discontinuity at the defect location, the difference Δf depends on the control parameter Re (Figs. 6b, c or 7b, c), this is different from δf, observed between right and left traveling rolls. No similar discontinuous behavior was observed for the average wavenumber.

For each defect location, the frequency discontinuity Δf gives the number of defects per time unity. We have verified experimentally that Δf is the inverse of defects period. In the range $\mathrm{Re} \in [265; 285]$, two distinct defects locations can be observed in the system, each one associated with a frequency discontinuity (Fig. 7). In this case, we consider Δf of the whole pattern as the sum of the discontinuities around each defect location.

The presence of defects destroys the correlation of the pattern: in fact, the correlation length fluctuates in time while the correlation time varies from a point to the other and is minimum at defect locations (Fig. 8).

3.2 Amplitude holes in the secondary modulated pattern

For $\mathrm{Re} > \mathrm{Re_m} = 292 \pm 2$, a secondary instability of the traveling roll pattern occurs, yielding a spatio-temporal modulation of the pattern with a wavelength of approximately three rolls. This supercritical transition and the resulting *triplet pattern* have been extensively studied in [22]. In particular, it has been mentioned that, for $\mathrm{Re} > \mathrm{Re}^\star \approx 308$, the triplets exhibit defects (collisions of triplets with loss of one triplet). The triplet collisions are very similar to the primary roll collisions, and sometimes coexist with the latter. Figure 9 shows a collision of triplets, followed by a strong distorsion of the pattern. The demodulation of the reflected light intensity signal, with filters centered around the roll mode (q_1, ω_1) gives access to the local wavenumber of the rolls, which is the traveling wave of the triplet pattern, resulting from the roll wavenumber oscillation [22]. Demodulation of this roll wavenumber signal, with filters centered around the triplet mode (q_2, ω_2) yields the local properties of the triplets, *i.e.* amplitude, spatial and temporal phase gradients (Figs. 10 and 11). The amplitude $|A_2(x,t)|$ of roll wavenumber signal represents the triplets amplitude. It shows a strong dip propagating in the pattern associated with a phase jump; this localized object is called an *amplitude hole*. The amplitude holes appear spontaneously in the triplet pattern and relax with life-time varying from 0.5 to 2.5. The holes propagate with velocity $v_\mathrm{h} \approx 10$, in a direction opposite to that of triplets [21]. We have observed that the number of defects and holes increases with the control parameter although no quantitative data are available. The appearance of defects and holes in the triplet pattern is responsible for a sharp increase of the phase noise in the system [22].

4 Discussion

4.1 Pattern envelope

The traveling roll pattern observed in the Taylor-Dean system occurs *via* a supercritical Hopf bifurcation and can be represented by the following signal:

$$u(t,x) = A(t,x)\mathrm{e}^{\mathrm{i}(\omega_r t - qx)} + B(t,x)\mathrm{e}^{\mathrm{i}(\omega_l t + qx)} + \text{c.c.} \quad (2)$$

where c.c. stands for complex conjugate. The amplitudes $A(t,x)$ and $B(t,x)$ of the right and left traveling waves are described by two coupled complex Ginzburg-Landau equations [1,5]:

$$\tau_0\left[\frac{\partial A}{\partial t} + v\frac{\partial A}{\partial x}\right] = \epsilon(1+\mathrm{i}c_0)A + \xi_0^2(1+\mathrm{i}c_1)\frac{\partial^2 A}{\partial x^2} - g(1+\mathrm{i}c_2)|A|^2 A - \delta(1+\mathrm{i}c_3)|B|^2 A \quad (3)$$

$$\tau_0\left[\frac{\partial B}{\partial t} - v\frac{\partial B}{\partial x}\right] = \epsilon(1+\mathrm{i}c_0)B + \xi_0^2(1+\mathrm{i}c_1)\frac{\partial^2 B}{\partial x^2} - g(1+\mathrm{i}c_2)|B|^2 B - \delta(1+\mathrm{i}c_3)|A|^2 B \quad (4)$$

where τ_0 is the characteristic time of the roll pattern, ϵ is the reduced control parameter of the bifurcation defined previously, v is the group velocity of traveling rolls, and ξ_0 is the coherence length of the pattern. The coefficients c_i $(i = 0, 1, 2, 3)$ are related to the linear $(i = 0, 1)$ and nonlinear $(i = 2, 3)$ dispersion of waves. Since the bifurcation is supercritical, the saturation constant $g > 0$. The constant δ describes the competition between left and right traveling waves: if $0 < \delta << g$, the two waves can exist on the pattern and there is a tendency to generate a standing wave, while for $\delta >> g$, a local development of a wave cancels the other at the same location and one obtains a propagating wave in one direction. In our case, we have observed rolls traveling to the left and to the right separated by a source, we therefore have the situation with $\delta >> g$.

The amplitude vanishes at the edges of the pattern and no reflection has been observed, so the boundary conditions for the equation are $[A(x=0) = A(x=L) = 0,$

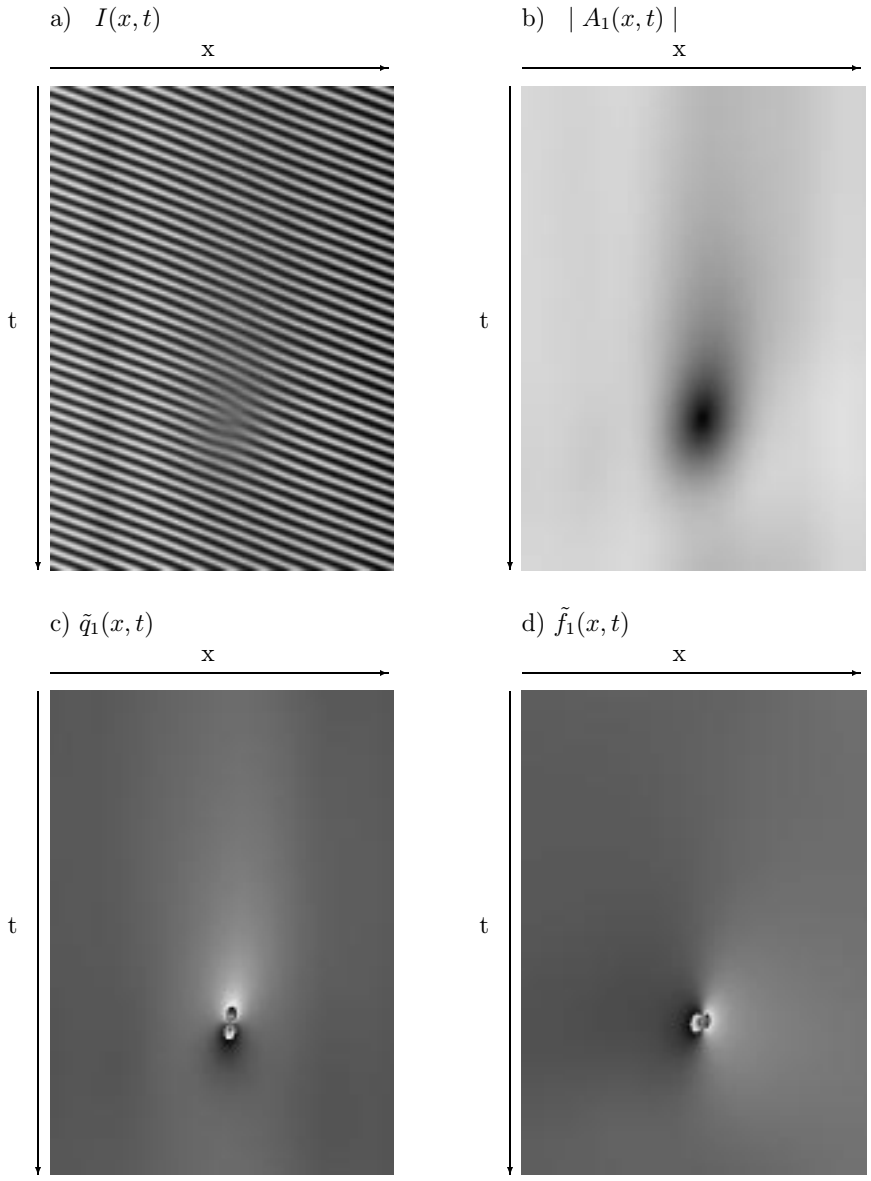

Fig. 4. Space-time diagram of the primary pattern (a), the wave amplitude (b in arbitrary units), wavenumber (c) and frequency (d) around a point defect at Re = 283. The pattern is shown over a time extension of 1.9 and a spatial extension of 13.

$B(x = 0) = B(x = L) = 0$]. Therefore, we will consider each edge as a *sink*[1]. In the source, the amplitude of each wave decreases down to zero. From the amplitude profiles, we have determined a coherence length for each amplitude drop or growth near the edges and the source. For this purpose, we have represented the amplitude of traveling roll pattern without point defects as a combination of hyperbolic tangent functions (which are particular solutions of the stationary Ginzburg-Landau equation) [23,24]:

$$A(x) = \frac{1}{4}A_0 \left(1 - \tanh \frac{x - x_{\rm er}}{\sqrt{2}\xi_{\rm er}}\right)\left(1 + \tanh \frac{x - x_{\rm sr}}{\sqrt{2}\xi_{\rm sr}}\right) (5)$$

$$B(x) = \frac{1}{4}B_0 \left(1 + \tanh \frac{x - x_{\rm el}}{\sqrt{2}\xi_{\rm el}}\right)\left(1 - \tanh \frac{x - x_{\rm sl}}{\sqrt{2}\xi_{\rm sl}}\right) (6)$$

where subscripts l and r refer to left and right respectively, e and s refer to edge and source. The values of the coherence length ξ and positions x given in Table 1 for few values of the control parameter Re have been obtained by fitting the amplitude profiles to the functions (5) and (6). From this table, we have found that the values of coherence length for both edges are approximately the same and so are those for the two waves in the source, moreover, they decrease with the control parameter Re. The coherence length $\xi_{\rm s}$ defines the size of the source and indicates the range of the interaction between the right and left traveling waves. The measured values of ξ indicate a disymmetry between the source and the sink (edge).

[1] A more precise definition of source and sink is related to the sign of the nonlinear group velocity of perturbations [28,29].

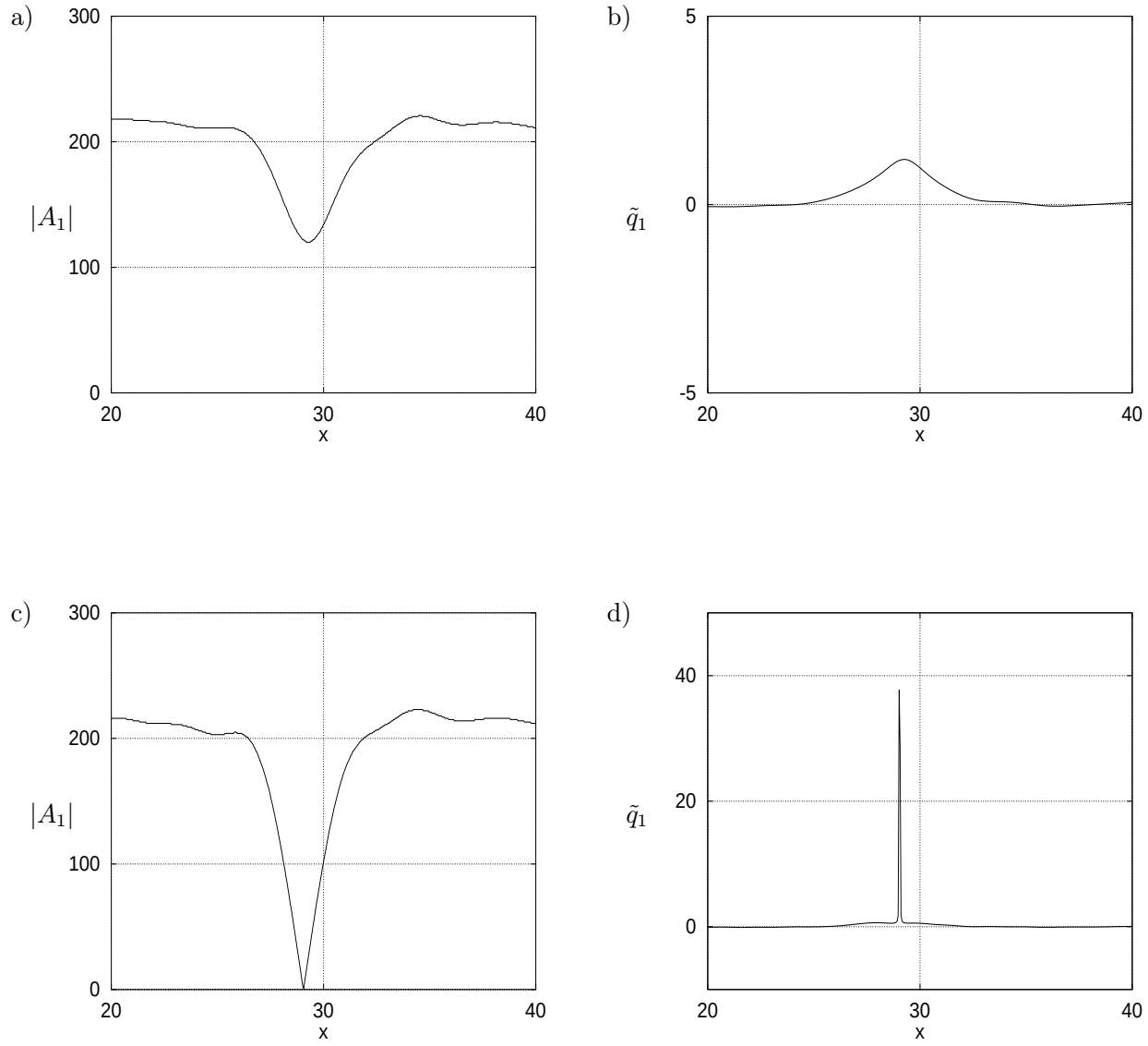

Fig. 5. Spatial profile of the amplitude (a and c) and the wavenumber (b and d) at Re = 283 before a defect ($t - t_c = 0.4$) and at the instant of a defect ($t - t_c \to 0^-$), where t_c is the date of the defect.

Table 1. Coherence length near source and sinks (edges).

Re	left				right			
	edge		source		source		edge	
	x_{le}	ξ_{le}	x_{ls}	ξ_{ls}	x_{rs}	ξ_{rs}	x_{re}	ξ_{re}
270	14.4	1.41	25.9	2.40	31.2	2.62	71.7	1.41
273	8.0	1.48	23.5	1.70	26.1	1.84	70.0	1.63
279	6.6	1.13	26.7	1.56	25.5	1.48	75.0	1.06

From the evolution of the coherence lengths, we can determine the associated characteristic length ξ_0, defined by $\xi = \xi_0 \epsilon^{-\frac{1}{2}}$: near the edges (sinks), $\xi_{0e} = 0.28 \pm 0.04$ and near the source $\xi_{0s} = 0.39 \pm 0.05$. The effect of the pattern edges (sinks) is strong for small values and decreases for higher values of the control parameter ϵ, leading to a stable pattern with respect to longwavelength modulations. Hence no defect is observed for $\epsilon \simeq 0.1$. The coherence length of the source is larger than that of the edge ("sink"). Similar results have been reported in experimental study of traveling waves induced by a hot wire below a free surface of a liquid [25] although with a different scaling ($\xi \sim \epsilon^{-1}$). Our results and those of Vince-Dubois are in a qualitatively good agreement with theoretical studies of traveling waves in one-dimensional system. In fact, these studies have indicated that sources are wider than sinks and that the presence of sources and sinks induces a wavenumber selection in the bulk of the pattern [26,27,29].

4.2 Defects

In the experimental run described in this paper, the source was stabilized near the left edge, and defects occur in the right traveling roll wave (with larger

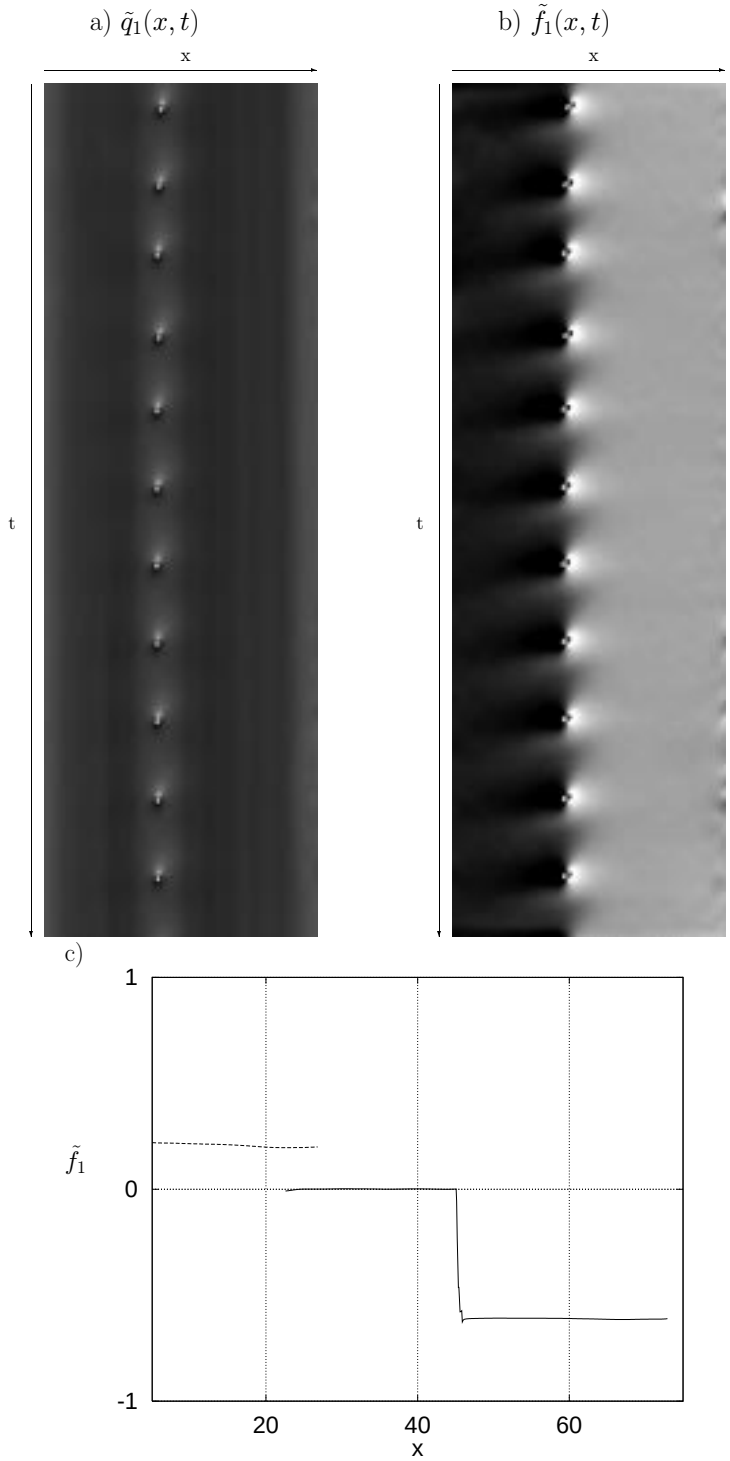

Fig. 6. Space-time diagram of the wavenumber (a) and frequency (b) for the right traveling wave at Re = 283. The pattern is shown over a time extension of 18.1 and a spatial extension of 46.3.; c) Time-averaged frequency profile for right (solid line) and left (dashed line) traveling waves. A source is present at $x = 24.9$ and point defects at $x = 45.4$.

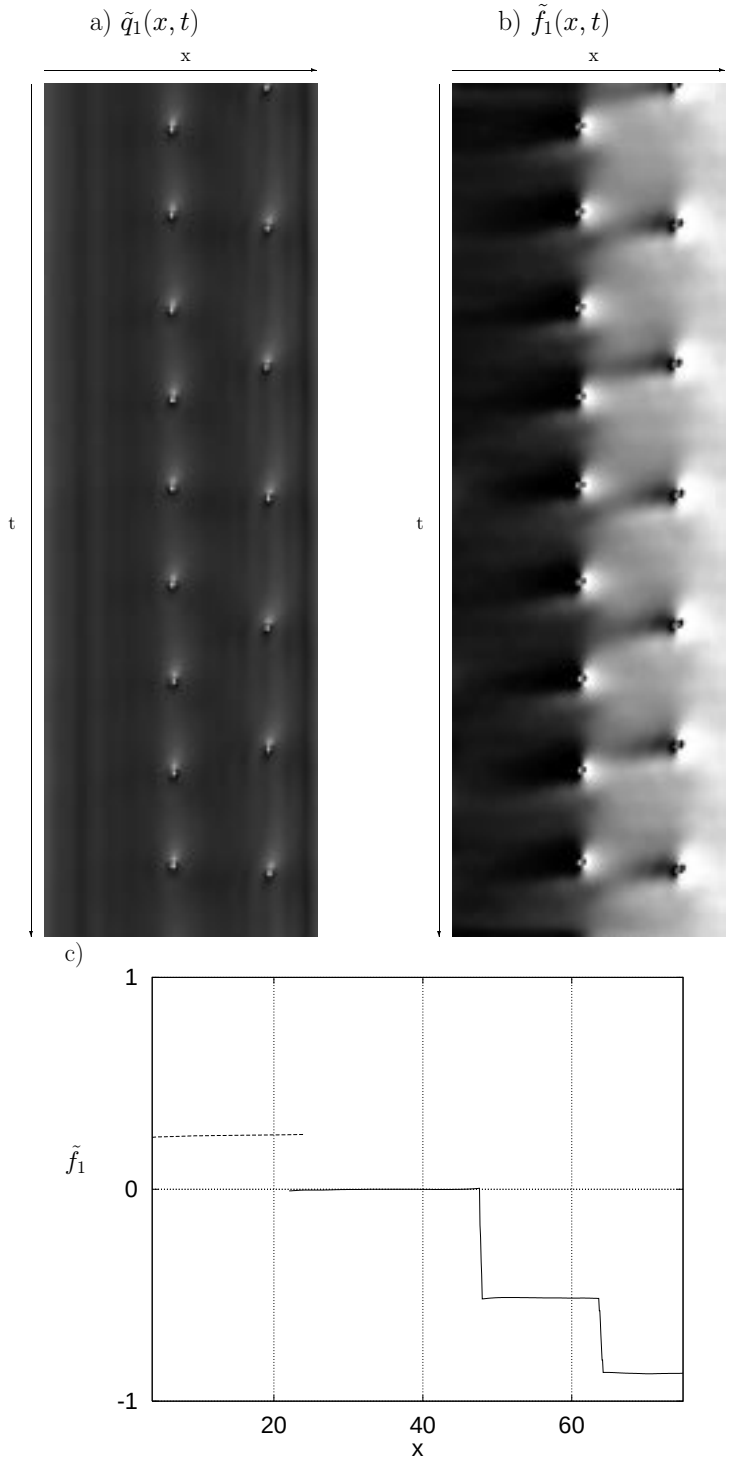

Fig. 7. Space-time diagram of the wavenumber (a) and frequency (b) for the right traveling wave at Re = 276. The pattern is shown over a time extension of 18.1 and a spatial extension of 46.3. c) time-averaged frequency profile for right (solid line) and left (dashed line) traveling waves. A source is present at $x = 24.1$ and point defects at $x = 47.8$ and $x = 63.9$.

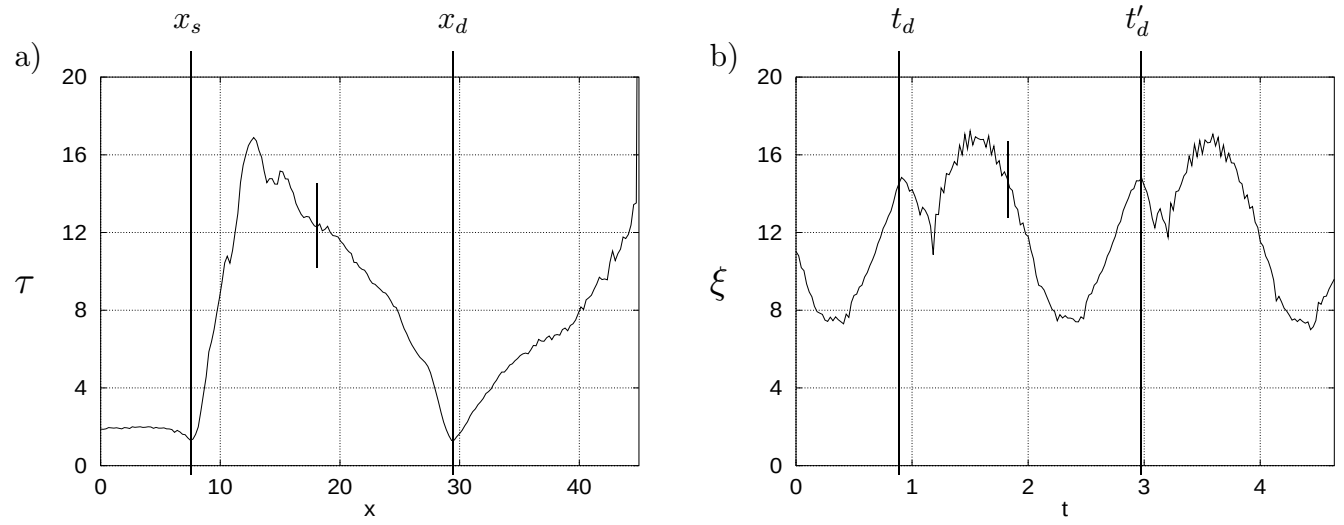

Fig. 8. a) Correlation time in the presence of a source at x_s and a point defect at x_d, and b) correlation length in the presence of point defects at t_d and t'_d, at $\mathrm{Re} = 283$.

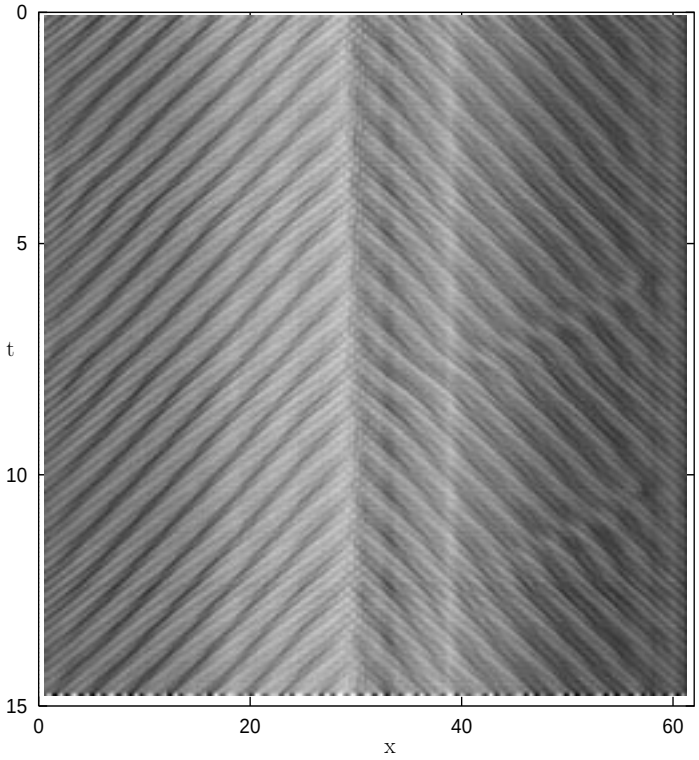

Fig. 9. Space-time diagram of the pattern at $\mathrm{Re} = 312$.

extension). Therefore, far from the source, the description of the defects dynamics can be done in the framework of one Ginzburg-Landau equation for the amplitude A, setting $B = 0$ in (3). For pattern in extended system, the complex Ginzburg-Landau equation possesses linearly stable states (plane waves) and "turbulence " states separated by the Benjamin-Feir line $1 + c_1c_2 = 0$ in the plane (c_1, c_2). Dynamical states found in the region $1 + c_1c_2 < 0$ are classified into defect turbulence, phase turbulence, bichaotic and intermittent states [9]. We may comment our results in the light of recent numerical solutions of this equation [8,9].

A defect occurs as a collision of two rolls and is due to an accumulation of phase gradient due to longwavelength modulations in the pattern. The vanishing amplitude and the phase jump of 2π around the defect are the characteristics of topological defects observed in most of spatio-temporal patterns in extended systems. They are singular solutions of the complex Ginzburg-Landau equation [7].

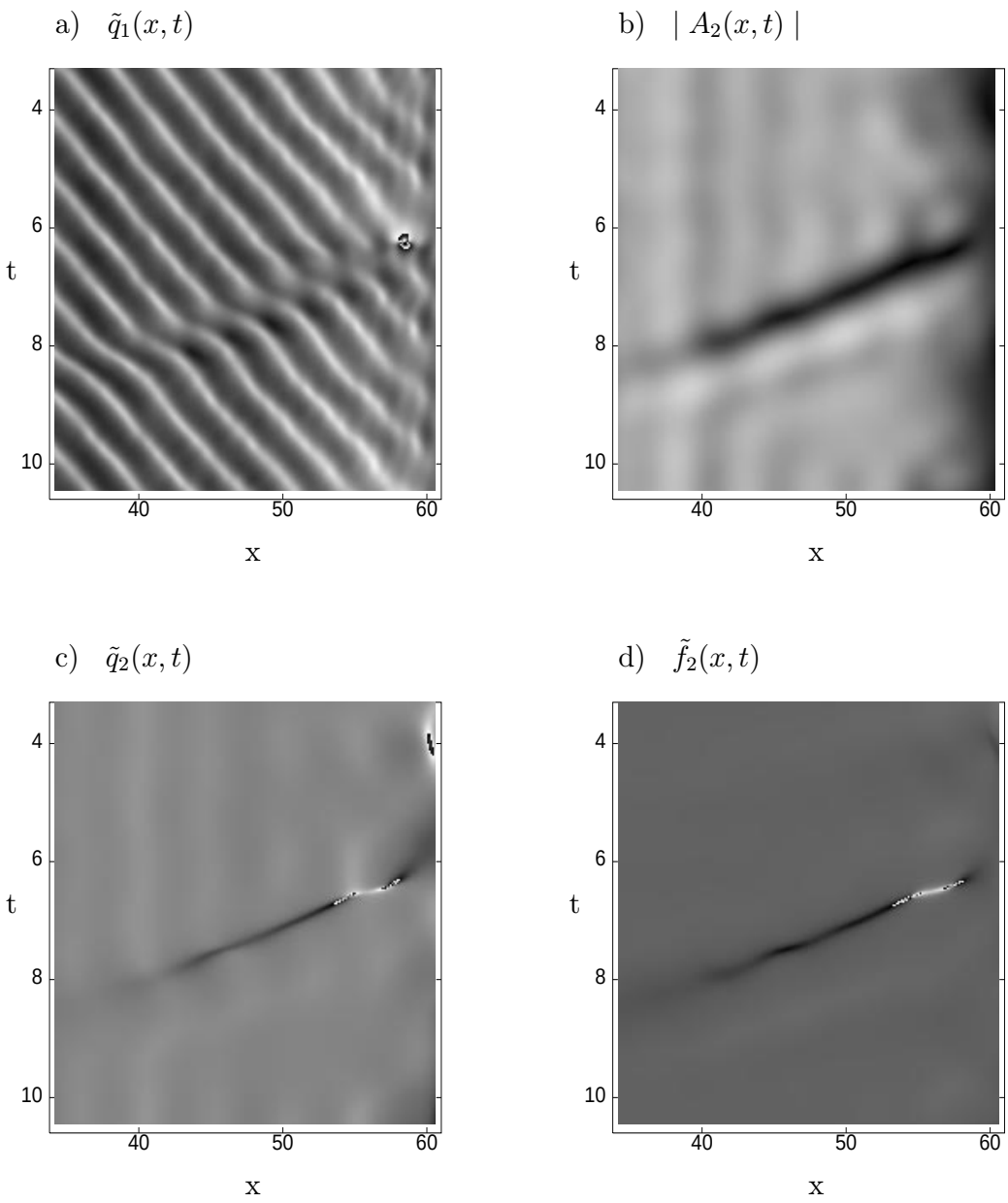

Fig. 10. a) Space-time diagram of the roll wavenumber at Re = 312. Space-time diagrams of the triplet amplitude (b), wavenumber (c) and frequency (d) at Re = 312.

4.2.1 Defects periodicity

The regularity observed in defects nucleation is related to the pattern frequency inhomogeneity. In fact, we have seen that the amplitude profiles are not symmetric for each wave and that the coherence lengths in the source and sink are different. This disymmetry imposes a frequency difference near the source and that near a sink according to the relation [12] $\omega = \frac{1}{\tau_0}[\epsilon(c_0 - c_2) - \xi_0^2 Q^2(c_1 - c_2)]$ where Q is the wavenumber of longwavelength modulations. Hence, the frequency difference acts as a forcing of defects nucleation, and fixes the time between two consecutive defects. This time has a lower bound imposed by the propagation time of roll in the pattern $T_{\min} = L/v = 2$, where L is the sub-pattern length (spatial range of the frequency gradient) and v is the roll drift velocity. If Δf is higher than $1/T_{\min}$, then the pattern produces two positions of defects in order to adapt to this constraint. The frequency profile has then two steps corresponding to each defect position (Fig. 7). If L is short, the frequency remains homogeneous in space and no collision can occur, this is the case in the left subpattern (Figs. 2 and 3).

The measure of the phase instability of the whole pattern Δf is a function of the control parameter Re (Fig. 12):

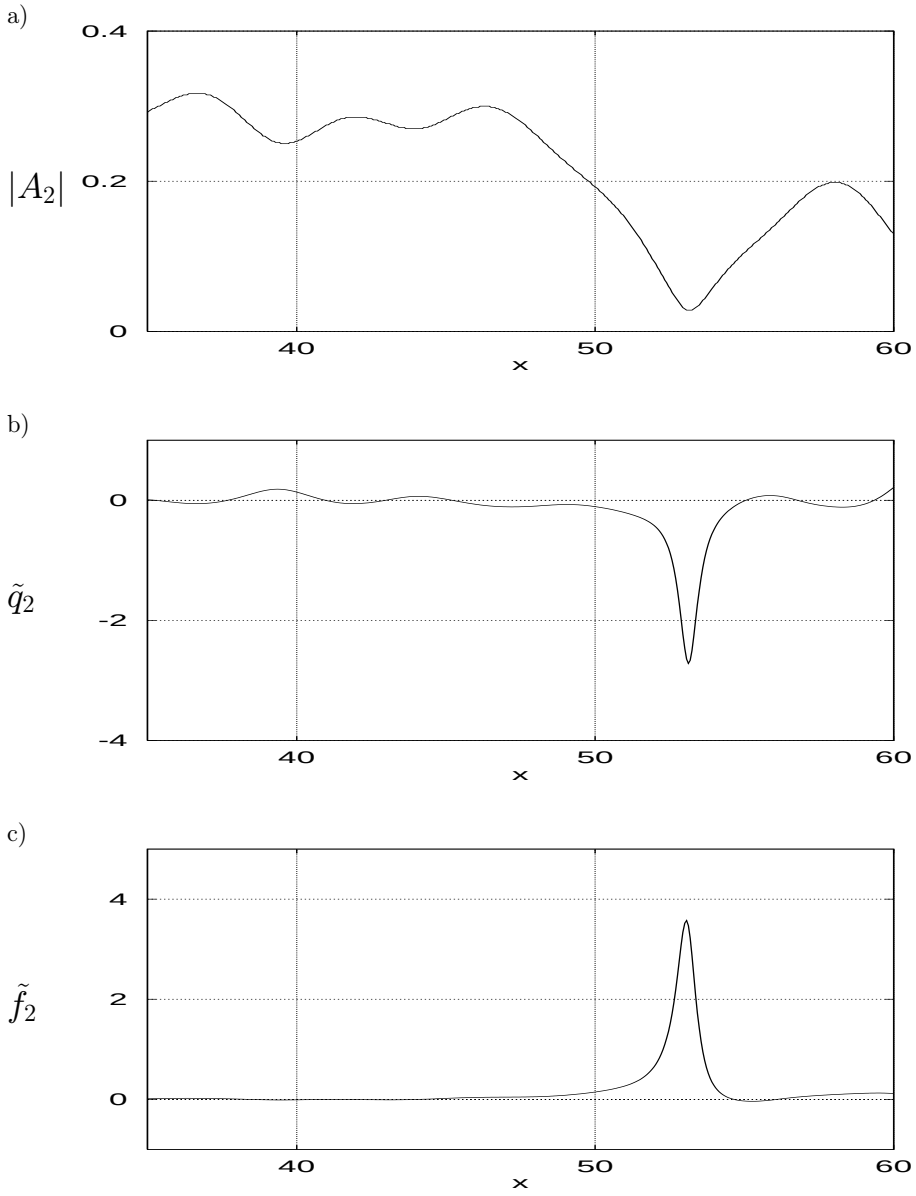

Fig. 11. Spatial profile of the triplet amplitude (a), wavenumber (b) and frequency (c) around an amplitude hole at Re = 312.

it is minimum at the boundaries of the phase instability domain, and maximum for Re $\sim$ 270, with approximately 1 defect per time unity.

4.2.2 Diffusive regime and defect core

We are interested in the neighborhood of defect locations before and after roll collision. We may distinguish two regimes in the nucleation of a defect: a diffusive regime, for $2T/3 < t_c - t < 0.3$, where the phase gradient remains smooth and the amplitude varies weakly; and a core regime, for $|t - t_c| < 0.3$, where the phase gradient and the amplitude vary drastically. Here t_c corresponds to the date of the collision (Fig. 4).

We call *diffusive* the regime in which the pattern is subject to long-wavelength phase modulations that may be described, by a truncated phase diffusion equation of the form [6,17,30]:

$$\frac{\partial \tilde{q}}{\partial t} = D\frac{\partial^2 \tilde{q}}{\partial x^2} \tag{7}$$

where $\tilde{q} = \partial\Phi/\partial x - \bar{q}$ is the perturbation from the average wavenumber $\bar{q}$ and D is the phase diffusion coefficient

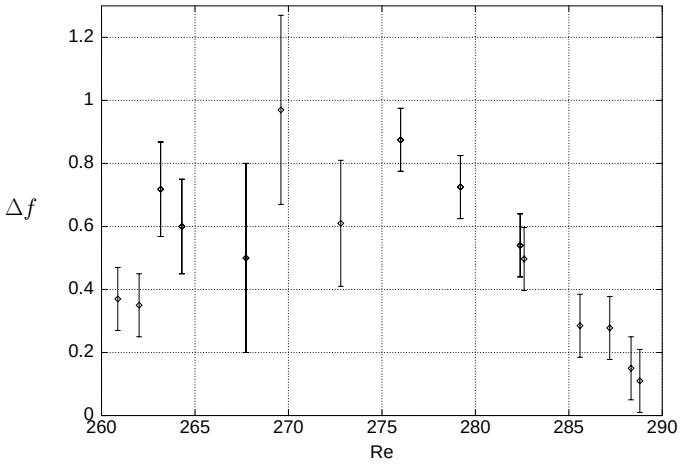

Fig. 12. Frequency difference between the source and the right edge of the pattern as a function of the control parameter.

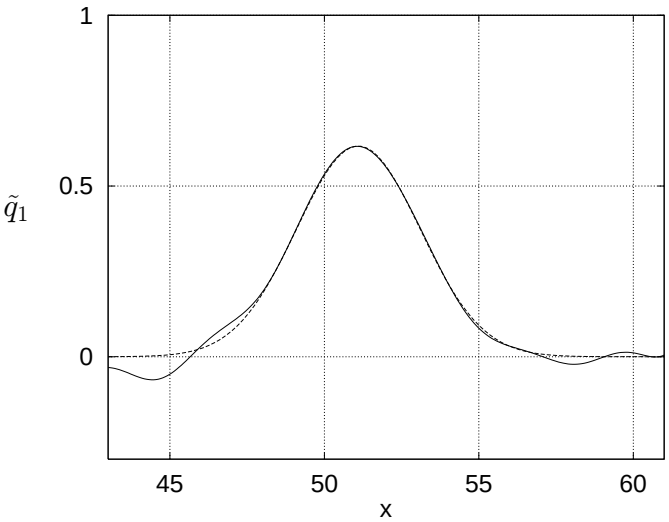

Fig. 13. Spatial profile of the wavenumber in the diffusive regime at $t - t_c = -0.56$, at Re = 282: experimental data (solid line), Gaussian fit (dashed line).

which, for traveling roll pattern, is given by

$$D = \frac{\xi_0^2}{\tau_0}(1 + c_1 c_2).$$

The occurrence of defects in our system for $260 < \mathrm{Re} < 288$ is a signature of a phase unstable pattern, in agreement with the Eckhaus-Benjamin-Feir condition $1+c_1c_2 < 0$. Each profile $\tilde{q}(x)$ of the phase gradient has been fitted by a Gaussian solution of diffusion equation (7) for different values of t (Fig. 13):

$$\tilde{q} \sim \mathrm{e}^{-\frac{x^2}{4Dt}}. \tag{8}$$

From the width of the Gaussian profile $\sigma = \sqrt{4Dt}$, we have estimated the phase diffusion coefficient D in the neighborhood of each defect. The obtained data are gathered in Figure 14 for different values of the control parameter: all values of D are negative, there is an accumulation of phase gradient in the point where the defect will nucleate. The existence of two different values of D in the same pattern with two defects locations, suggests that this coefficient is a local characteristic of the pattern. The diffusion coefficient can be related to the frequency inhomogeneity. In fact, the diffusion coefficient D varies linearly with the frequency difference Δf, as is shown in Figure 15. The slope of the curve $D(\Delta f)$ is homogeneous to the square of a length, which is characteristic of the phase perturbations and is found to be equal to 3 approximately. This length is close to the size of the triplets: the secondary structures of the pattern resulting from a phase modulation of the rolls [22]. A diffusive relaxation regime ($D > 0$) is not observed after the collision. This suggests that the pattern remains always Eckhaus-Benjamin-Feir unstable, even after the roll annihilation, since the frequency inhomogeneity forces a new defect nucleation. The point defects are generated by pattern dissymmetry between source and sink (edge), they induce phase perturbations

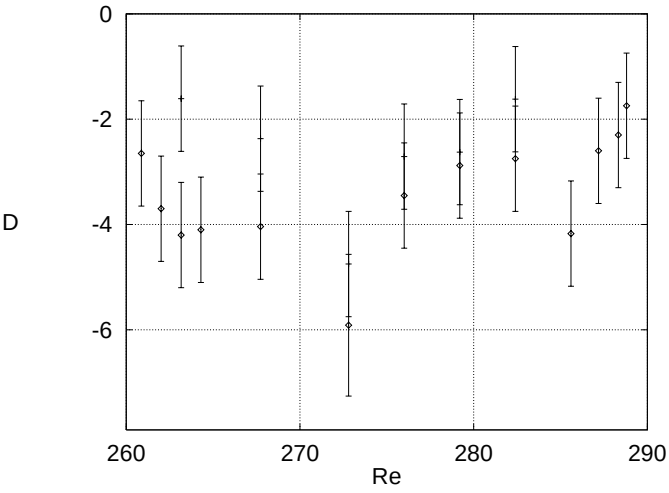

Fig. 14. Phase diffusion coefficient as a function of the control parameter. One value is obtained per defect location.

that allow us to measure the diffusion coefficient D without any need of external excitation. If the pattern does not contain defects, the method cannot be used and an external forcing of the pattern might be necessary [31,32].

In the core of the defect, the behavior of the phase is no more diffusive: the phase gradient increases drastically and its peak becomes very narrow like a Dirac function $\delta(x)$ (Fig. 5d). It can be described not by the truncated phase equation but by the complete Kuramoto-Sivashinski phase equation, which is known to exhibit shock-like solutions [4]. After the nucleation of defect, the phase gradient becomes a deep well that relaxes rapidly. We have measured the maximum of the phase gradient for $|t-t_c| < 0.3$,

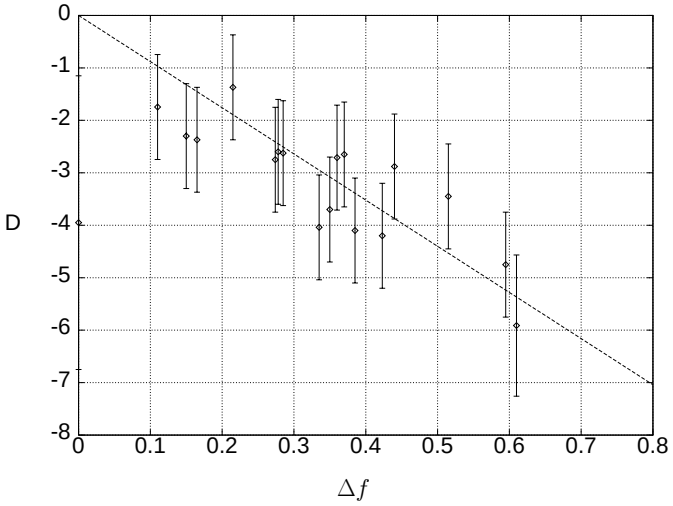

Fig. 15. Phase diffusion coefficient as a function of the frequency difference for each defect location.

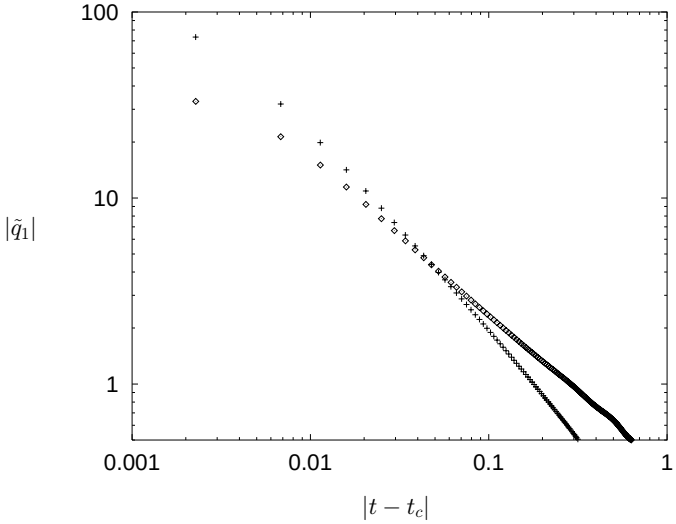

Fig. 16. Power-law increase of the wavenumber approaching a defect at Re = 287 ($\diamond$: before the defect, +: after the defect).

it follows a power law behavior (Fig. 16) of the form:

$$\tilde{q}(x_c) \sim (t_c - t)^{-a} \text{ for } t < t_c$$
$$\tilde{q}(x_c) \sim (t - t_c)^{-b} \text{ for } t > t_c. \quad (9)$$

We have determined the exponents a and b around 22 point defects in the range where they exist: Re $\in [261; 288]$. The mean and rms values measured are $a = 0.87 \pm 0.07$, and $b = 1.15 \pm 0.07$. There is no significant variation neither with the control parameter nor with the time between consecutive defects. The fact that $b > a$ indicates that the perturbation after collision relaxes faster than it has grown before, as can be seen in Figure 4.

4.3 Amplitude holes

In our experiment, the amplitude holes appear in a strongly modulated pattern which is a secondary instability mode. They are a result of roll collision or triplet collision. Such collisions that occur at large scale in comparison with those between rolls, induce a strong perturbation that propagates in the modulated pattern of triplet and strongly deforms it. A collision of triplets is a phase instability of the triplet pattern. In the difference with roll collisions in the primary pattern, the triplet collisions are not periodic in time and occur in erratic locations and so they cannot be related to frequency inhomogeneity of the pattern. The amplitude holes differ from the actual topological defect in the sense that the amplitude does not vanish in the core, and the phase jump does not reach 2π. The holes that we observe propagate in the opposite direction to that of the triplets, and are associated to a negative phase gradient (expansion of the pattern). The triplet collisions and amplitude holes induce a large background noise in the pattern and are the signature of the occurrence of the chaotic or intermittent regime of pattern in our system [22].

Amplitude holes have also been observed in a secondary oscillatory pattern in an annular convection cell [7,18] and in hydrothermal waves [33]. In these experiments, holes travel in the same direction as the wave and are associated to a positive phase gradient(compression of the pattern).

The amplitude holes have been found in theoretical and numerical studies of the complex Ginzburg-Landau equation in the Benjamin-Feir unstable and in the intermittency regimes [7–11,13]. A significant difference in the wavenumber between both sides of the hole is not detected in our experiment. This suggests that these holes are closer to the homoclinic solutions found by van Hecke [13], than the heteroclinic holes of the Nozaki-Bekki type [10,11].

5 Conclusion

We have studied the dynamics of defects in the roll pattern observed in the Taylor-Dean system, when only the inner cylinder is rotating. Using complex demodulation technique, we have measured the amplitude profiles of the traveling waves and determined, for each line defect, coherence lengths that show a disymmetry between source and sinks. This disymmetry, in a traveling pattern, induces a frequency inhomogeneity that leads to the periodic generation of roll collisions (defects). The periodic nucleation of defects could be described by including a periodic forcing in the Kuramoto-Sivashinski equation (this is left for a further detailed study). Two different dynamic behaviors have been identified in the neighborhood of each defect: a diffusive and a core region. In the diffusive region, we have measured a negative phase diffusion coefficient. In the core of defect, we established a power law behavior of the phase gradient in time with exponents independent of the control parameter. We have observed traveling amplitude holes in the strongly modulated triplet pattern. The observed states containing defects and holes belong to the Benjamin-Feir unstable domains obtained in recent numerical simulations of the complex Ginzburg-Landau equation.

The authors would like to thank A. Chiffaudel, P. Manneville and O. Cadot for fruitfull discussions during this work. We thank the referee for having provided us with recent theoretical works on CGLE. One of us (P.B.) benefited with a scolarship of MENRS. This work was partly supported by a grant from DRET.

References

1. P. Manneville *Structures dissipatives chaos et turbulence*, Aléa Saclay, CEA (1991).
2. T. Passot, A.C. Newell, Physica D **74**, 301 (1994).
3. Y. Estrin, L. Kubin, Rev. Phys. Appl. **23**, 1997 (1988).
4. Y. Kuramoto, *Chemical oscillations, waves and turbulence* (Springer-Verlag, 1984), Vol. 19.
5. M. Cross, P.C. Hohenberg, Rev. Mod. Phys. **65**, 851 (1993).
6. D. Walgraef, *Spatio-temporal pattern formation* (Springer-Verlag, New York, 1997).
7. J. Lega, B. Janiaud, S. Jucquois, V. Croquette, Phys. Rev. A **45**, 103 (1992).
8. H. Chaté, Nonlinearity **7**, 185 (1994).
9. R. Montagne, E. Hernández-Garcia, M. San Miguel, Phys. Rev. Lett. **77**, 267 (1996).
10. K. Nozaki, N. Bekki, Phys. Rev. Lett. **51**, 2171 (1983).
11. K. Nozaki, N. Bekki, J. Phys. Soc. Jap. **53**, 1581 (1984).
12. H. Sakaguchi, Prog. Theor. Phys. **85**, 417 (1991).
13. M. van Hecke, Phys. Rev. Lett. **80**, 1896 (1998).
14. P. Kolodner, Phys. Rev. A **46**, 6431 (1992).
15. P. Kolodner, Phys. Rev. A **46**, 6452 (1992).
16. I. Mutabazi, J.J. Hegseth, C.D. Andereck, J.E. Wesfreid, Phys. Rev. Lett. **64**, 1729 (1990).
17. B. Janiaud, A. Pumir, D. Bensimon, V. Croquette, H. Richter, L. Kramer, Physica D **55**, 269 (1992).
18. J.M. Flesselles, V. Croquette, S. Jucquois, Phys. Rev. Lett. **72**, 2871 (1994).
19. N. Mukolobwiez, Ph.D. thesis, University of Paris XI, France, 1998.
20. I. Mutabazi, J.J. Hegseth, C.D. Andereck, J.E. Wesfreid, Phys. Rev. A **38**, 4652 (1988).
21. P. Bot, Ph.D. thesis, University of Le Havre, France, 1998.
22. P. Bot, O. Cadot, I. Mutabazi, Phys. Rev. E **58**, 3089 (1998).
23. Y. Pommeau, S. Zaleski, J. Phys. France **42**, 515 (1981).
24. M. Tinkham, *Introduction to the Theory of Superconductivity* (R.E. Krieger Publishing Company, Inc., 1985).
25. J.M. Vince, M. Dubois, Europhys. Lett. **20**, 505 (1992).
26. W. van Saarloos, P.C. Hohenberg, Physica D **56**, 303 (1992).
27. P. Coullet, T. Frisch, F. Plaza, Physica D **62**, 75 (1993).
28. R. Alvarez, M. van Hecke, W. van Saarloos, Phys. Rev. E **56**, R3106 (1997).
29. M. van Hecke, C. Storm, W. van Saarloos, Elsevier preprint (1999).
30. Y. Liu, E. Ecke, Phys. Rev. Lett. **78**, 4391 (1997).
31. J.E. Wesfreid, V. Croquette, Phys. Rev. Lett. **45**, 634 (1980).
32. M.M. Wu, C.D. Andereck, Phys. Rev. A **43**, 2074 (1991).
33. J. Burguete, H. Chaté, F. Daviaud, N. Mukolobwiez, Phys. Rev. Lett. **82**, (1999).